Planetary and Space Science 73 (2012) 318–326

Contents lists available at SciVerse ScienceDirect

Planetary and Space Science

journal homepage: www.elsevier.com/locate/pss

Titan's photochemical model: Further update, oxygen species, and comparison with Triton and Pluto

Vladimir A. Krasnopolsky *

[a] Department of Physics, Catholic University of America, Washington, DC 20064, USA
[b] Moscow Institute of Physics and Technology, Dolgoprudnyy, Russia

ARTICLE INFO

Article history:
Received 4 May 2012
Received in revised form
7 August 2012
Accepted 10 August 2012
Available online 24 August 2012

Keywords:
Titan
Triton
Pluto
Atmospheres, Composition
Photochemistry
Evolution

ABSTRACT

My photochemical model for Titan's atmosphere and ionosphere is improved using the Troe approximation for termolecular reactions and inclusion of four radiative association reactions from those calculated by Vuitton et al. (2012). Proper fitting of eddy diffusion results in a reduction of the mean difference between 63 observed mixing ratios and their calculated values from a factor of 5 in my previous models for Titan to a factor of 3 in the current model. Oxygen chemistry on Titan is initiated by influxes of H_2O from meteorites and O^+ from magnetospheric interactions with the Saturn rings and Enceladus. Two versions of the model were calculated, with and without the O^+ flux. Balances of CO, CO_2, H_2O, and H_2CO are discussed in detail for both versions. The calculated model with the O^+ flux agrees with the observations of CO, CO_2, and H_2O, including recent H_2O CIRS limb observations and measurements by the Herschel Space Observatory.

Major observational data and photochemical models for Triton and Pluto are briefly discussed. While the basic atmospheric species N_2, CH_4, and CO are similar on Triton and Pluto, properties of their atmospheres are very different with atomic species and ions dominating in Triton's upper atmosphere and ionosphere opposed to the molecular composition on Pluto. Calculations favor a transition between two types of photochemistry at the CH_4 mixing ratio of $\sim 5\times 10^{-4}$. Therefore Triton's current photochemistry is still similar to that at the Voyager flyby despite the observed increase in N_2 and CH_4. The meteorite H_2O results in precipitation of CO on Triton and CO_2 on Pluto near perihelion.

1. Introduction

My self-consistent photochemical model for Titan's atmosphere and ionosphere (Krasnopolsky 2009, 2010; hereafter Kr09 and Kr10) is a convenient tool to study atmospheric chemical composition on Titan and to test various hypotheses related to the chemical composition. Using the N_2 and CH_4 densities near the surface, the model calculates vertical profiles of 83 neutral species and 33 ions up to 1600 km. The model computes radiative transfer based on the aerosol observations from the Huygens probe and gaseous absorptions calculated interactively. The self-consistent nature of the model is advantageous compared to partial models that are aimed at simulating just a few atmospheric species. Those models require a background atmosphere that is generally poorly known and neglect effects of the calculated species on the background atmosphere.

2. Versions of the model

My models of Titan's photochemistry are aimed to simulate the global mean conditions, that is, the solar zenith angle is $z=60^\circ$ and the solar photon flux is for the medium solar activity and half that at Titan's heliocentric distance to account for the night side. The model results are therefore applicable to the low latitudes or to globally averaged data.

Both the Voyager 1 flyby and the Cassini/Huygens mission refer to the southern summer in the 30-years annual cycle of Titan. The CIRS observations demonstrate very strong latitudinal variations of the atmospheric species at 100–400 km. Eight years have passed since the beginning of the observations, and some seasonal trends have become available as well. However, the seasonal and latitudinal variations are not the subject of my modeling. Observational data that are used for comparison with my models are collected in Table 1.

The GCMS abundances of CH_4 and Ar are applied as the lower boundary conditions, while the H_2 fraction may be computed with the models. Vertical profiles of nine species at 150–300 or 150–400 km are taken from the CIRS limb observations at 5°N (Vinatier, 2010), and values at the boundaries are compared with

* Corrresponding author at: Catholic University of America, Department of Physics, 6100 Westchester Park Dr. #911, College Park, MD, Washington, DC 20064, USA. Tel.: +1 240 473 6831.
E-mail address: vlad.krasn@verizon.net

0032-0633/$ - see front matter © 2012 Elsevier Ltd. All rights reserved.
http://dx.doi.org/10.1016/j.pss.2012.08.013

Table 1
Summary of the observational data on Titan's chemical composition (mixing ratios).

h (km)	0[a]	150[b]	300[b]	400[b]	1050[c]	1400[d]	1100[e]
CH_4	0.057	0.015[a]	–	–	0.022	0.11	–
Ar	$3.4-5$[f]	–	–	–	1.3–5	–	–
H_2	1.0–3	–	–	–	$3.4-3$	0.02	–
C_2H_2	–	3–6	3–6	2–6	3.4–4	–	–
C_2H_4	–	1.5–7	3–8	–	3.9–4	–	1–3
C_2H_6	–	1–5	1.4–5	1.7–5	4.6–5	–	–
C_3H_4	–	1–8	1–8	–	9.2-6	–	–
C_3H_6	–	–	–	–	2.3–6	–	–
C_3H_8	–	1.3–6	1–6	5–7	2.9–6	–	–
C_4H_2	–	2–9	6–9	8–9	5.6–6	–	1–5
C_6H_2	–	–	–	–	–	–	8–7
C_6H_6	–	$2-10$[g]	–	–	2.5–6	–	3–6
C_7H_4	–	–	–	–	–	–	3–7
C_7H_8	–	–	–	–	2.5–8	–	2–7
NH_3	–	–	–	–	–	–	7-6
CH_2NH	–	–	–	–	–	–	1–5
HCN	–	2.5–7	5–7	3–7	2.5–4	–	2–4
CH_3CN	–	$6-9$[h]	$1.4-8$[h]	$3-8$[h]	–	–	3–6
C_2H_3CN	–	–	–	–	3.5–7	–	1–5
C_2H_5CN	–	–	–	–	1.5–7	–	5–7
HC_3N	–	1–11	1–9	–	1.5–6	–	4–5
C_4H_3N	–	–	–	–	–	–	4–6
HC_5N	–	–	–	–	–	–	1–6
C_5H_5N	–	–	–	–	–	–	4–7
C_6H_3N[i]	–	–	–	–	–	–	3–7
C_6H_7N[i]	–	–	–	–	–	–	1–7
C_2N_2	–	$2-10$[j]	–	–	2.1–6	–	–
H_2O[k]	–	$7-11$[l]	$3-10$[m]	–	1.2–5	–	–
CO	–	4.7–5	–	–	–	–	–
CO_2	–	2–8	1.8–8	3–8	–	–	–

[a] GCMS (Niemann et al., 2010).
[b] CIRS limb (Vinatier, 2010) at 5 °N.
[c] INMS (Magee et al., 2009).
[d] INMS (Cui et al., 2009).
[e] Derived from INMS ion spectra (Vuitton et al., 2007).
[f] $3.4–5=3.4\times10^{-5}$.
[g] CIRS nadir (Coustenis, 2010), low latitudes.
[h] IRAM results at 170, 300, and 400 km (Marten et al., 2002).
[i] Our model does not involve this species.
[j] At ~100 km and 5–30°N (from Fig. 9 in Teanby et al. (2009)).
[k] Mean of CIRS (Cottini et al., 2012) and Herschel (Moreno et al., 2012) observations.
[l] At 100 km.
[m] At 250 km.

the models. Mixing ratios of C_6H_6 and C_2N_2 from the CIRS nadir observations near the equator, the CH_3CN profile from the IRAM data, mean H_2O abundances from the CIRS and Herschel observations, and the CO value from De Kok (2007) are included in Table 1 (27 values at $h<500$ km to evaluate the model results).

The next set of data (20 values) is the summary of the INMS neutral species observations near 1050 km (Magee et al., 2009) and 1400 km (Cui et al., 2009). Finally, Vuitton et al. (2007) fitted the INMS T5 ion spectrum at 1100 km by a model with numerous abundances of neutrals as free parameters. The best fit fractions are given in Table 1 as well (18 values, and C_6H_3N and C_6H_7N are not involved in our models). Overall, 63 observed mixing ratios from Table 1 will be used for comparison with our models.

Kr09 evaluated a mean difference between a model and observations by a difference factor

$$F=\exp\left(\frac{1}{n}\sum_{i=1}^{n}|\ln(f_i/f_{i0})|\right)$$

Here f_i and f_{i0} are the calculated and observed mixing ratios. F is equal to one if a model perfectly fits the observations; if F is, say, 3, then a mean difference between a model and observations is a factor of 3. Evidently the difference factor is not a perfect tool to estimate quality of a model: apart the calculated abundances, it is important how they have been calculated. However, it is convenient for comparison of our models with 63 observed mixing ratios in Table 1.

Kr09 and Kr10 suggest three versions of the model. Model 1 is a version with hydrodynamic escape of light species (molecular mass $\mu\le18$) according to Strobel (2009). Eddy diffusion K in Model 1 has three breakpoints at 100, 400, and 700 km with $K=3\times10^4$, 10^5, and 10^8 cm^2 s^{-1}, respectively. K is constant below 100 km and above 700 km and varies linearly between the breakpoints in the log scale. Difference factors for this model (Table 2) show a good agreement with both sets of the INMS data, while the calculated vertical profiles below 500 km are much steeper than those observed on the limb by CIRS.

To reduce vertical gradients in the calculated mixing ratios below 500 km, Hörst et al. (2008) proposed eddy diffusion increasing as n^{-2} (n is the atmospheric number density) from $K=400$ cm^2 s^{-1} below 70 km to 3×10^7 cm^2 s^{-1} above ~300 km. (A similar but less steep profile of K was adopted in the model by Lavvas et al. (2008).) A model with this eddy diffusion was given in Appendix to Kr09. Improvements in the difference factors below 500 km (Table 2) are compensated by some deterioration in the upper atmosphere.

Model 3 was calculated in Kr10 assuming no hydrodynamic escape from Titan (Johnson et al. 2009). According to Yelle et al. (2008), the required eddy diffusion in the thermosphere is equal to $(4\pm3)\times10^9$ cm^2 s^{-1} to agree the CH_4 and Ar densities observed by INMS and GCMS (Niemann et al. 2010) in the upper and lower atmospheres, respectively, without hydrodynamic escape. The minimum value of 10^9 cm^2 s^{-1} was adopted in Model 3. Another change in Model 3 is an increase in the ammonia production by reactions

$$NH+H_2CN\rightarrow HCN+NH_2$$

$$NH_2+HCN\rightarrow HCN+NH_3$$

the latter suggested by Yelle et al. (2009). These reactions reduce but cannot remove a significant difference between the INMS observations of ammonia and its model abundances. Difference factors for Model 3 (Table 2) are slightly worse than those for the models with hydrodynamic escape. However, this cannot be considered as a strong argument in favor of hydrodynamic escape on Titan.

Below we will make some improvements in the model, consider in more detail the chemistry of oxygen species on Titan, and compare the model results with recent observations of H_2O on Titan. Then we will discuss some effects of oxygen chemistry on Triton and Pluto.

3. Termolecular reactions

Rates of the termolecular reactions A+B+M→AB+M are equal to k_0[A][B][M] at low pressure and k_∞[A][B] at high pressure.

Table 2
Difference factors of the models relative to the observations in Table 1.

Model	$h<500$ km	INMS	INMS*	Total
Lavvas et al. (2008)	4.30	4.49	16.1	5.63
Kr09	9.18	2.52	3.70	4.83
Kr09, Appendix	6.65	3.09	6.61	5.21
Kr10	9.28	3.01	4.65	5.45
This model	**3.91**	**2.35**	**3.21**	**3.16**

Kr09 and Kr10 are Krasnopolsky (2009, 2010), respectively. All my models in this table include influxes of H_2O and O^+. INMS is from columns 6 and 7 and INMS* from column 8 in Table 1. 46 mixing ratios from Lavvas et al. (2008) and 63 mixing ratios from each of my models are compared with the observations in Table 1.

Here k_0 ($cm^6\ s^{-1}$) is the low pressure limit for the reaction rate coefficient, and k_∞ ($cm^3\ s^{-1}$) is the high pressure limit. We applied

$$k=\frac{k_0}{1+(k_0/k_\infty)[M]}=\frac{k_0}{1+([M]/M_\infty)}\ \text{and}\ M_\infty=\frac{k_\infty}{k_0}$$

in Kr09 and Kr10. Here M_∞ has the dimension of number density, and the rate coefficient fits both low and high pressure limits in this formulation.

A more accurate approximation for the rate coefficient at intermediate pressures was obtained by Troe:

$$k=\frac{k_0}{1+(k_0/k_\infty)[M]}\times 0.6^{(1+X^2)^{-1}}\ \text{and}\ X=lg\left(\frac{k_0}{k_\infty}[M]\right)$$

We upgraded our model using the Troe approximation, though the effect from this improvement is insignificant.

Vuitton et al. (2012) suggested another approximation:

$$k=\frac{k_0[M]X+k_r}{1+((k_0[M]X)/k_\infty)}$$

Here k_r is the rate coefficient of radiative association and X is a parameter that is determined by some complicated relationships. The approximation fits the high pressure limit but does not fit the low pressure limit, because e.g. $X\approx 50$ for very small [M] in the reaction $H+CH_3+M\rightarrow CH_4+M$. The relationships for X are given without any proof and explanation and overall do not conform the definition of the low pressure limit. Therefore we will not use the suggested approximation and the calculated low and high pressure limits for ten reactions in Vuitton et al. (2012). Radiative association reactions from that paper are discussed below.

4. Radiative association reactions

We checked effects of the radiative association reactions calculated by Vuitton et al. (2012) on the results of our model. Four of the ten reactions,

$$H+C_2H_4\rightarrow C_2H_5+h\nu \qquad k_1=9\times10^{-16}\,T^{-0.53}\,e^{-19/T}=5.4\times10^{-17}\ cm^3\ s^{-1}\ \text{at 170 K} \quad (1)$$

$$H+C_4H_2\rightarrow C_4H_3+h\nu \qquad k_2=8.7\times10^{-20}\,T^{2.75}\,e^{-50/T}=9\times10^{-14}\ cm^3\ s^{-1}\ \text{at 170 K} \quad (2)$$

$$H+C_4H_3\rightarrow C_4H_4+h\nu \qquad k_3=1.8\times10^{-4}\,T^{-3}\,e^{-162/T}=6\times10^{-16}\ cm^3\ s^{-1}\ \text{at 170 K} \quad (3)$$

$$H+C_6H_5\rightarrow C_6H_6+h\nu \qquad k_4=1.6\times10^{-10}\ cm^3\ s^{-1}\ \text{at 170 K} \quad (4)$$

affect the calculated abundances and have been included in the model. The most significant and unexpected effect is from reaction (2) that diminishes C_2H_6 above 900 km and enhances C_2N_2. This reaction initiates a cycle

$$H+C_4H_2\rightarrow C_4H_3+h\nu$$

$$C_4H_3+CH_3\rightarrow C_4H_2+CH_4$$

$$\text{Net}\ H+CH_3\rightarrow CH_4$$

This cycle reduces densities of methyl CH_3 and therefore ethane C_2H_6.

Another unexpected consequence of reactions (1–4) is the increase of the cyanogen abundance that is formed by

$$CN+CH_2\rightarrow C_2N_2+CH_2$$

$$N+CHCN\rightarrow C_2N_2+H$$

in our model. These species are controlled by H via

$$CH_2CN+H+M\rightarrow CH_3CN+M$$

$$CHCN+H\rightarrow C_2N+H_2$$

A significant reduction of H in the radiative associations results in an increase in C_2N_2. Both changes in C_2H_6 and C_2N_2 better agree with the INMS observations. Reaction (4) facilitates the production of benzene and also helps to fit the INMS observations (Table 1).

Kr09 and Kr10 adopted loss of species i by condensation near and below the tropopause as $L_{ic}=A\ \ln S_i$. Here $S_i=n_i/n_{is}$ is the supersaturation of i species. Yung et al. (1984) applied $L_i=AS_i/(1+S_i)\approx A$ because typically $S_i\gg 1$. They adopted $A=10^{-9}\ s^{-1}$ without any discussion, and we will use this A in our model.

5. Eddy diffusion and improved photochemical model

We discussed in Section 2 that the steep increase in eddy diffusion $K=A/n^2$ in the stratosphere helps to fit the vertical profiles of species observed by CIRS on the limb (Tables 1 and 2). However, a more traditional profile of K with a break near 700–800 km and a constant value above is favorable for the INMS observations. Here we will try to combine both profiles to get the best difference factors.

Similar to Kr09 and Kr10, eddy diffusion is given by three break points and therefore six parameters: the breakpoint altitudes $h0$, $h1$, and $h2$ and values $K0$, $K1$, and $K2$. Eddy diffusion is equal to

$$K=\frac{K1}{1+(K1/K0)\times(n/7.5\times10^{17})^2}$$

between $h0$ and $h1$. It is constant below $h0$, increases to $K2$ at $h2$ linearly in the log scale, and is constant above $h2$. All values are chosen to minimize the difference factor. The best fit parameters are 61, 536, and 790 km and 2300, 3.2×10^5, and $6.5\times10^8\ cm^2\ s^{-1}$, respectively. The calculated profile of eddy diffusion is shown in Fig. 1a along with the temperature profile and the calculated N_2 densities. $K=190\ cm^2\ s^{-1}$ below 60 km, the profiles of K and D are rather close above 500 km, and the homopause $D=K$ is at 1000 km. The difference factor of the model is 3.16, better than 5.45 for the model in Kr10 (Table 2).

The calculated profiles of CH_4, H_2, Ar, and C_2H_x hydrocarbons are shown in Fig. 1b; seven other abundant hydrocarbons and seven nitriles are exposed in Fig. 1c and d, respectively. The profiles in Fig. 1 may be compared with the observational data in Table 1.

Mean dayside ($z=60^\circ$) density profiles of the most abundant ions are given in Fig. 2a–c. The ionospheric peak with $e_{max}=3650\ cm^{-3}$ is at 1070 km. Cassini radio occultations at $z=87^\circ$ resulted in $e_{max}=2000\ cm^{-3}$ at 1200 km (Kliore et al., 2008). According to Cravens et al. (2005), the peak altitude moves up by ~140 km from $z=59^\circ$ to 90° while the peak electron density reduces by a factor of 2. Therefore both the calculated peak density and its altitude in our model are in excellent agreement with the radio occultation observations. However, INMS measured a peak sum of all ions of $1800\ cm^{-3}$ at 1100 km during the dayside Cassini flyby T40 on January 5, 2008, at 12°S and $z=38^\circ$ (Westlake et al., 2012). This peak electron density is even smaller than that observed at $z=87^\circ$ and disagrees with both radio occultations and our model. Two other instruments, Langmuir probe and CAPS-IBS, measured $e_{max}\approx 2800\ cm^{-3}$ at 1120 km in the T40 flyby (Westlake et al., 2012). This value is closer to the model prediction. The nighttime flyby T5 with a strong precipitation of magnetospheric electrons is therefore better for comparison of models with the INMS observations (Vuitton et al., 2007). Those measurements were modeled by Vuitton et al. (2007), Cravens et al. (2009), and Kr09;

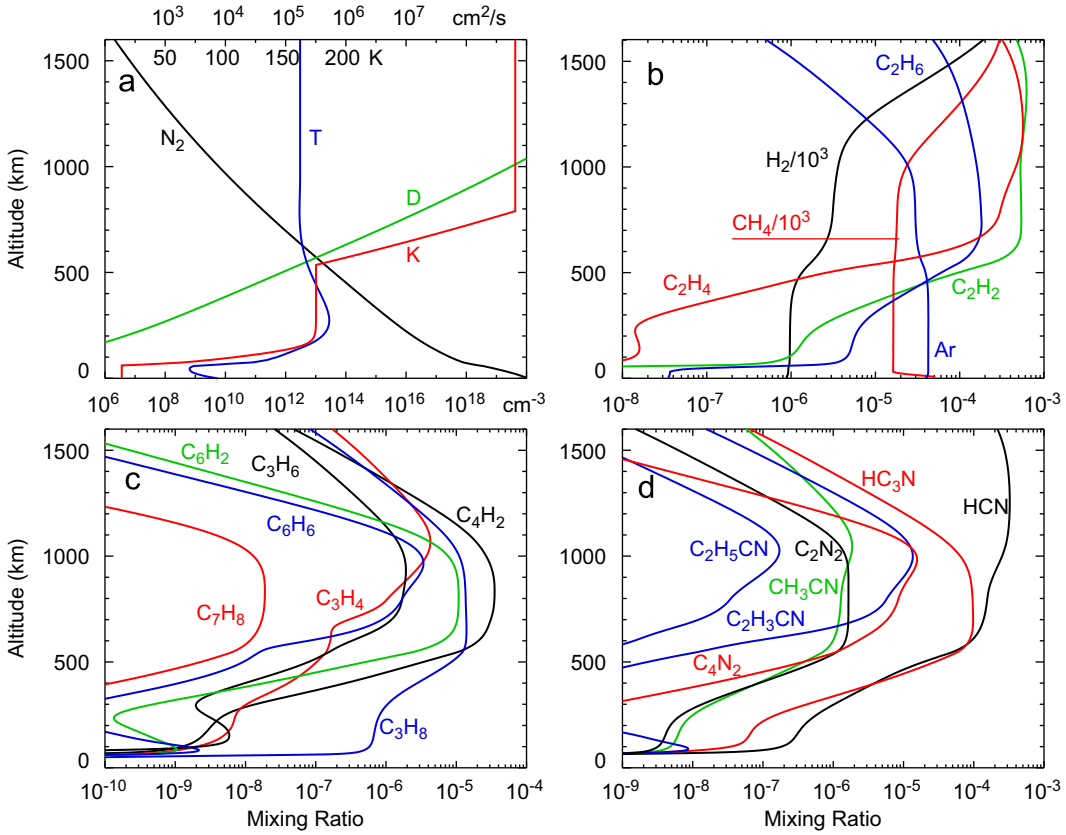

Fig. 1. Initial data and calculated vertical profiles of neutral species in the model: (a) profiles of temperature, N_2 density, eddy and molecular (CH_4 in N_2) diffusion; (b) CH_4, H_2, Ar, and C_2H_x hydrocarbon; (c) some other abundant hydrocarbons; (d) the most abundant nitriles.

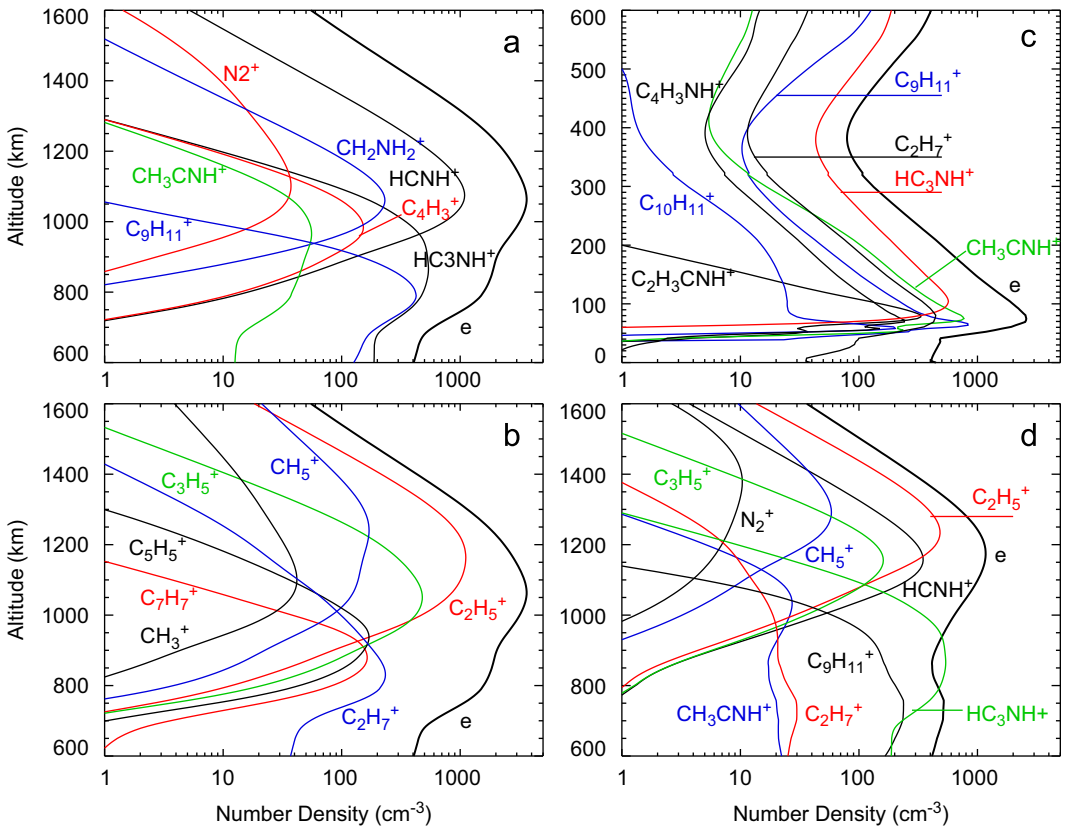

Fig. 2. Ion composition in the daytime ionosphere above (a, b) and below (c) 600 km. The nighttime ionosphere (d) is calculated for the conditions of the T5 flyby with strong precipitation of magnetospheric electrons.

the difference factors are 1.74, 3.88, and 2.01, respectively (Table 7 in Kr09), and 2.15 for the current model (Fig. 2d). The abundances of 18 neutral species were fitting parameters in the model by Vuitton et al. (2007). Both neutral and ion compositions are calculated interactively in our models, and the difference factor obtained may be considered as very good.

6. Oxygen species

6.1. Observations

Oxygen species were first discovered on Titan by ground-based observations that revealed a significant abundance of CO (Lutz et al. 1983). Later CO was measured using ground-based infrared and microwave instruments and by the Voyager/IRIS and Cassini/CIRS. A summary of the observations may be found in De Kok (2007) and Hörst et al. (2008), and the mean CO (Fig. 3) is close to the CIRS value of 47 ± 8 ppm (De Kok, 2007). CO_2 was detected by IRIS, ISO, and CIRS (see Hörst et al. (2008)), and the CIRS limb profiles at 5°N from Vinatier et al (2010) is also shown in Fig. 3.

H_2O was detected by the Infrared Space Observatory (Coustenis et al. 1998) using its rotational lines near 40 μm. The measured mole fraction was equal to 8^{+6}_{-4} ppb at ~400 km (Fig. 3) obtained by scaling of the H_2O profile from a model by Lara et al. (1996) to fit the observed emissions. Recently water vapor was observed by the Herschel Space Observatory using its rotational lines in the far infrared and submillimeter ranges. The retrieved H_2O vertical profile is

$$f_{H_2O} = 2.3 \times 10^{-11} \left(\frac{12.1 mbar}{p}\right)^{0.49}$$

(Moreno et al., 2012). This profile is given in Fig. 3 in the altitude range of 80 to 300 km. A detailed study of the CIRS nadir and limb spectra reveals H_2O as well (Cottini et al., 2012), and the derived abundances are shown in Fig. 3. The INMS observations resulted in 4–34 ppm of H_2O at a mean altitude of 1077 km (Cui et al., 2009).

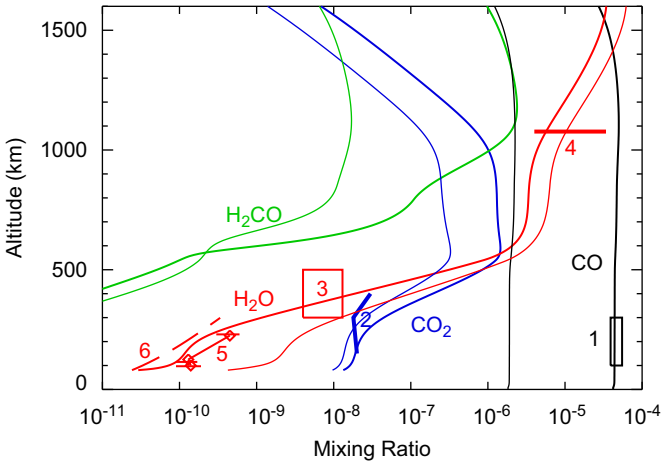

Fig. 3. Main oxygen species on Titan: observations and the model. Solid lines show the model with both meteorite influx of H_2O and magnetospheric flux of O^+. Thin lines show the model without flux of O^+. Observations: (1) CIRS (De Kok, 2007), (2) CIRS at 5 °N (Vinatier, 2010), (3) ISO (Coustenis et al. 1998), (4) INMS (Cui, 2009), (5) CIRS (Cottini et al., 2012), and (6) Herschel (Moreno et al. 2012).

6.2. Previous models

Previous full photochemical models for Titan's atmosphere that involved the oxygen chemistry (Yung et al., 1984; Toublanc et al., 1995, Lara et al., 1996, Banaszkiewicz et al., 2000, Wilson and Atreya, 2004) adopted a meteorite influx of H_2O and fixed the CO mixing ratio near the surface. The oxygen chemistry on Titan was studied in more detail by Wong et al. (2002) and Hörst et al. (2008).

Wong et al. (2002) applied the model by Yung et al. (1984) with updated kinetic data from Moses et al. (2000). Using the study by Pereira et al. (1997), they argued that a basic reaction of the CO production in the previous models, $OH + CH_3 \rightarrow CO + 2H_2$, does not proceed, and H_2O recycles after the photolysis via $OH + CH_3 \rightarrow H_2O + {}^1CH_2$. They adopted an H_2O influx of 1.5×10^6 cm^{-2} s^{-1} and calculated a CO abundance of 1.8 ppm with no sources of CO at the surface or from space, much lower than the 47 ppm observed. A CO influx of 1.1×10^6 cm^{-2} s^{-1} was required to fit the observed CO.

Hartle (2006) analyzed the Voyager and Cassini/CAPS data and found a magnetospheric influx of O^+ on Titan with a rate of $\sim 10^6$ cm^{-2} s^{-1}. These ions of atomic oxygen may originate from Saturn's ring and Enceladus. Hörst et al. (2008) calculated a model for the oxygen species on Titan using the influxes of OH and O and eddy diffusion as fitting parameters. Their best model is for $\Phi_O = 1.6 \times 10^6$ cm^{-2} s^{-1}, $\Phi_{OH} = 2.6 \times 10^6$ cm^{-2} s^{-1}, and eddy diffusion discussed in Section 2 for Model 2. Hörst et al. (2008) achieved an excellent agreement with the observations of CO, CO_2, and H_2O available at that time. However, the calculated H_2O abundances were ~0.1, 2, and 2.3 ppb at 100, 200, and 300 km, respectively, that is, exceeding the recent measurements above 100 km.

6.3. Oxygen species in our models

Kr09 and Kr10 keep the basic ideas of the oxygen chemistry from Wong et al. (2002) and Hörst et al. (2008) with some changes. We assumed no influx of CO from the surface and space. Kr09 proved that the metastable oxygen states $O(^1D)$ and $O(^1S)$ may be neglected because of the low production and the strong quenching by N_2. Five species (HOCO, CH_3COCH_3, CH_2CO, CH_3OH, and $HOCH_2CH_2$) in Hörst et al. (2008) were assumed to ultimately produce either CO_2 or CO. We concluded that two of those (HOCO, CH_3COCH_3, and also CH_3O) may be neglected as well and add photolyses of CH_2CO and CH_3OH to balance their production. The production of $HOCH_2CH_2$ is balanced by the reaction with H in our model. Overall, we reduced the numbers of oxygen species and reactions from 14 and 44 in Hörst et al. (2008) to 12 and 31, respectively (Table 3). 10 species and 21 reactions are similar to those in Hörst et al. (2008), and 1 species (CH_3COH) and 10 reactions were added and marked by asterisks in Table 3.

We approximated an H_2O flux profile from English et al. (1996) by

$$\frac{d\Phi_{H_2O}}{dh} = \frac{0.185}{ch\left(\frac{h-700}{50}\right)} = \frac{0.37}{\exp\left(\frac{h-700}{50}\right) + \exp\left(\frac{700-h}{50}\right)} \text{cm}^{-3}\ \text{s}^{-1}$$

Here *ch* is hyperbolic cosine, and *h* is in km. The H_2O flux is equal to 2.95×10^6 cm^{-2} s^{-1}; scaled to the surface, it is 4.78×10^6 cm^{-2} s^{-1}. This flux is within uncertainties of that observed on Saturn by Feuchgruber et al. (1997). The O^+ flux was chosen at 1.70×10^6 cm^{-2} s^{-1} at 1100 km and 3.46×10^6 cm^{-2} s^{-1} scaled to the surface.

These fluxes and the oxygen chemistry (Table 3) remain unchanged in all our models including that in this paper. The model in Kr09 (Appendix) with eddy diffusion from Hörst et al. (2008) showed CO, CO_2, and H_2O rather similar to those in Hörst

Table 3
Reactions of oxygen species in Titan's atmosphere.

#	Reaction	Yield (γ)/Rate coefficient	Column rate	h (km)
1	$CO+h\nu \rightarrow C+O$	predissociation, diss. ionization, electron impact dissociation	6717	1012
2	$H_2O+h\nu \rightarrow OH+H$	$\gamma=0.78$ 1.0 (110–145–200 nm)	1.03+7	569
3	$O+H_2$	$\gamma=0.22$, 0	9.62+4	835
4	$CO_2+h\nu \rightarrow CO+O$	–	2.56+5	404
5	$H_2CO+h\nu \rightarrow CO+H_2$	$6.4\times10-7$	1.10+6	763
6	$CO+2H$	2.1×10^{-7}	3.60+5	763
7	$HCO+H$	3.6×10^{-7}	6.17+5	763
8*	$CH_2CO+h\nu \rightarrow CO+CH_2^*$	2×10^{-6}	7.60+4	513
9*	$CH_3OH+h\nu \rightarrow H_2CO+H_2-$	–	3.11+4	494
10	$O+CH_3 \rightarrow H_2CO+H$	7×10^{-11}	2.03+6	1034
11	$CO+H_2+H$	6×10^{-11}	1.74+6	1034
12*	$O+C_2H_4 \rightarrow CH_3CO+H$	$\gamma=0.3$, $2.2\times10^{-17}\,T^{1.9}\,e^{-92/T}$	1.83+4	534
13*	CH_3+HCO	$\gamma=0.6$	3.66+4	534
14*	H_2CO+CH_2	$\gamma=0.1$	6098	534
15	$OH+CH_3 \rightarrow CH_2^*+H_2O$	$1.8\times10^{-8}\,T^{-0.91}\,e^{-275/T}$	4.41+6	653
16	H_2CO+H_2	$3.8\times10^{-14}\,T^{-0.12}\,e^{209/T}$	9348	653
17	$OH+CH_3+M \rightarrow CH_3OH+M$	$1.1\times10^{-10}\,T^{-6.21}\,e^{-671/T}$, 4×10^{15}	3.11+4	521
18	$OH+CH_4 \rightarrow CH_3+H_2O$	$2.5\times10^{-12}\,e^{-1775/T}$	1.14+6	504
19	$OH+CO \rightarrow CO_2+H$	$2.8\times10^{-13}\,e^{-176/T}$	4.35+6	503
20	$OH+H_2 \rightarrow H_2O+H$	$9\times10^{-13}\,e^{-1530/T}$	1.67+5	526
21	$OH+C_2H_2+M \rightarrow CH_3CO+M$	5.5×10^{-30}, 5×10^{16}	2.04+4	467
22	$OH+C_2H_4+M \rightarrow HOCH_2CH_2+M^6$	$1.4\times10^{-17}\,T^{-4.5}$, 10^{16}	2.14+5	553
23	$HCO+H \rightarrow CO+H_2$	1.8×10^{-10}	6.67+5	713
24	$HCO+CH_3 \rightarrow CH_4+CO$	9×10^{-11}	1.10+5	715
25*	$CH_3CO+H \rightarrow HCO+CH_3$	3.6×10^{-11}	1.24+5	529
26*	CH_2CO+H_2	1.9×10^{-11}	6.56+4	529
27	$CH_3CO+CH_3 \rightarrow CH_2CO+CH_4$	10^{-11}	1.08+4	436
28	$CO+C_2H_6$	4.8×10^{-11}	5.17+4	436
29*	$CH_2CO+H \rightarrow CO+CH_3$	1.3×10^{-15} T1.45 e−1400/T	403	320
30*	$CH_3COH+H \rightarrow CH_3CO+H_2$	7×10^{-15} T1.16 e−1210/T	2.14+5	508
31*	$HOCH_2CH_2+H \rightarrow CH_3COH+H_2$	3.3×10^{-11}	2.14+5	553
32	H_2O meteorite flux		4.78+6	704
33	O^+ influx		3.46+6	1103
34	H_2O condensation		6.13+4	<84
35	CO_2 condensation		4.08+6	<60

Rate coefficients of photolyses (in s^{-1}) are halves of the daytime values at $\lambda>200$ nm, those for two-body reactions are in $cm^3\,s^{-1}$, and termolecular rate coefficients are low-pressure limits (in $cm^6\,s^{-1}$) and limiting densities (ratios of high/low pressure limits at 170 K). References to the photolysis cross sections and reaction rate coefficients are given in Tables 3 and 4 in Kr09. Column rates are in $cm^{-2}\,s^{-1}$ and scaled to the surface (see Kr09); h is the reaction weighted-mean altitude for the model with the flux of O^+. Reaction marked by asterisks are lacking in Hörst et al. (2008). $4.16+6=4.16\times10^6$.

et al. (2008). Results of our current model with and without the O^+ flux are shown in Fig. 3, and the column reaction rates are in Table 3. We will consider first the case without the O^+ flux.

The H_2O photolysis branch that forms O (R3) is very weak because of the strong CH_4 absorption at $\lambda<140$ nm. There are three basic pathways for OH after photolysis of H_2O: (1) to restore H_2O in reactions with CH_3, CH_4, and H_2 (R15, 18, 20); (2) to form CO in reactions with CH_3, C_2H_2, and C_2H_4 (R16, 17, 21, 22) because the products in these reactions decompose further to CO; (3) to remove CO and form CO_2 in R19. Photolysis cross sections of CO_2 at 170–200 nm are smaller than those of H_2O in this range by a factor of $\sim$300; therefore photolysis of CO_2 is weak, and CO_2 mostly irreversibly condenses in our model. Photodestruction of CO is very slow (R1), and the CO abundance without the O^+ flux is determined by a balance between pathways (2) and (3) and equal to 1.9 ppm, similar to that in Wong et al. (2002). Its lifetime is very long, and CO/N_2 is constant throughout the atmosphere.

The mean altitude of CO_2 formation is 500 km (R19). Eddy diffusion is high above this altitude, and the CO_2 mole fraction is constant up to the homopause near 1000 km in this model with a further decrease (Fig. 3) because of diffusive separation with the large CO_2 molecular mass. CO_2 is decreasing below 400 km to the tropopause where it condenses. This decrease is partly compensated by eddy diffusion $K\approx An^{-2}$ to fit the CO_2 and some other CIRS limb observations (Vinatier, 2010). This increase in eddy diffusion is by a factor of 140 and from 60 to 200 km in our model, while it is by a factor of 70,000 from 100 to 300 km in Hörst et al. (2008).

The production of H_2O by meteorites (R32) and pathway (1) is balanced by the photolysis (R2-3) with a minor contribution from condensation (R34). The H_2O profile differs from that of CO_2 above the homopause due to diffusive separation with the low H_2O molecular mass. The H_2O decrease is steeper than CO_2 below 400 km because of the higher photolysis rate.

In the case of the O^+ flux (R33, $3.46\times10^6\,cm^{-2}\,s^{-1}$), it is completely spent to form CO in reactions (10–11) with CH_3. Each CO_2 photolysis event adds two CO molecules as well, because O is converted into CO. The reactions of pathway (2) give $2.75\times10^5\,cm^{-2}\,s^{-1}$, and the total CO production is $4.36\times10^6\,cm^{-2}\,s^{-1}$. It is balanced by the reaction with OH giving a CO mole fraction of 44 ppm, in accord with the observations and larger than that without the O^+ flux by a factor of 23. The CO mole fraction is constant up to $\sim$1200 km and decreases above this altitude because of diffusive enrichment in CH_4 and H_2.

The CO_2 production of $4.36\times10^6\,cm^{-2}\,s^{-1}$ in R19 CO+OH is balanced by its condensation (R35) and photolysis (R4). The calculated CO_2 mole fraction agrees with the observed profile below $\sim$300 km (Fig. 3).

The production of H_2O by OH in R15 and R18 with CH_3 and CH_4 becomes smaller because of the competing reaction with CO and equals $5.55\times10^6\,cm^{-2}\,s^{-1}$. Adding the meteorite production results in $1.03\times10^7\,cm^{-2}\,s^{-1}$ that is perfectly balanced by the

photolysis and condensation. The H_2O abundance is smaller than that without the O^+ flux due to the greater loss of OH in the reaction with CO.

The calculated H_2O profile (Fig. 3) is between the Herschel (Moreno et al., 2012) and CIRS (Cottini et al., 2012) observations. It intersects the square of the ISO observations (Coustenis et al., 1998) near the middle. The ISO value of 8^{+6}_{-4}=4–14 ppb near 400 km was obtained by scaling of the H_2O profile from Lara et al. (1996). Our H_2O profile equals to 8 and 14 ppb at 370 and 390 km, respectively, well within the ISO contribution function with a broad peak at 400 km. Furthermore, the ISO observation corresponds to an H_2O column of $\left(2.6^{+1.9}_{-1.6}\right)\times10^{14}$=(1.0–4.5)$\times10^{14}$ cm^{-2} above 100 km, and the model gives 4.7×10^{14} cm^{-2}, near the uncertainty of the observation. The H_2O model values are also within the scatter of the INMS measurements (Cui, 2009). We emphasize that the combination of the Herschel, CIRS, and ISO data with the INMS measurements requires a steep decrease in the H_2O fraction below 600 km, and this decrease is simulated by the model because of the significant effect of the H_2O photolysis.

Atomic oxygen reacts with methyl in the upper atmosphere and forms formaldehyde H_2CO. Therefore formaldehyde in the upper atmosphere is much more abundant in the case of the O^+ flux (Fig. 3). This source becomes small below 500 km where the calculated H_2CO profile is almost insensitive to the O^+ flux.

The CO lifetime is a ratio of its column abundance and its column loss rate in the reaction with OH and equals 75 Myr. This may be compared with chemical lifetimes of N_2 and CH_4 on Titan, 25 Byr and 21 Myr, respectively (Kr09). Lifetimes of the other photochemical products are very much shorter (Table 6 in Kr09).

Although CO is abundant on Titan, it forms photochemically and does not require a source on the surface. It cannot condense and deposit to the surface. Precipitation of H_2O ice is negligible as well, and that of CO_2 is 9 g cm^{-2} Byr^{-1}, that is, $\sim10^{-3}$ of the total precipitation (Kr10).

7. Comparison with Triton and Pluto

There are three bodies with the nitrogen-methane atmospheres in the Solar System: Titan, Triton, and Pluto. Titan is at$\sim$10 AU from the Sun, and its N_2 is completely in the atmosphere that is very dense. Triton and Pluto are at $\sim$30 AU from the Sun and have tenuous atmospheres that are in equilibrium with ices of N_2, CH_4, and CO. In addition to these ices, ices of CO_2, H_2O, and HCN have been detected on Triton (Burgdorf et al. (2010) and references therein) and C_2H_6 on Pluto (Merlin et al, 2010 and references therein).

7.1. Basic observational data

Triton was studied by the Voyager 2 flyby in 1989 (Broadfoot et al., 1989) that revealed vertical profiles of N_2, temperature, N (Krasnopolsky et al., 1993), and CH_4 (Herbert and Sandel 1991), atmospheric pressure of 13.5 μbar and an electron density profile in the ionosphere (Tyler et al., 1989), a surface temperature of 38 $\pm$ 3 K (Conrath et al., 1989), and haze and clouds (Pollack et al., 1990, Krasnopolsky et al., 1992).

Stellar occultations in 1995 and 1997 (Olkin et al., 1997, Elliot et al., 2000) showed a significant increase in the atmospheric pressure since the Voyager flyby. Finally, gaseous CH_4 and CO were detected (Lellouch et al., 2010) by ground-based high-resolution spectroscopy using the CRIRES spectrograph at the Very Large Telescope of the European South Observatory in Chile. The observed abundances are 0.08 $\pm$ 0.03 cm-atm of CH_4 and 0.3 cm-atm of CO, the latter with an uncertainty within a factor of 3. The N_2 abundance during the observations was generally unknown, and Lellouch et al. (2010) adopted 40 μbar combining the Voyager data and the stellar occultations. This abundance is equal to 410 cm-atm using Triton's gravity acceleration of 78 cm s^{-2}. The obtained mole fractions are given in Table 4 and compared with those in a photochemical model by Krasnopolsky and Cruikshank (1995) that was based on the Voyager results. The difference is well within the observation uncertainties. Methane varies with altitude on Triton and Pluto; henceforth its mixing ratio is a ratio of the column abundances of CH_4 and N_2.

Table 4
Observed mole fractions of CH4 and CO on Triton and Pluto and those in photochemical models.

	f_{CH4}[a]	f_{CO}	CO/CH_4
Triton, L10	$\sim2\times10^{-4}$	$\sim7\times10^{-4}$	3.7
Triton, KC95	10^{-4}	3×10^{-4}	3
Pluto, L11	$0.6^{+0.6}_{-0.3}$ %	$5^{+10}_{-2.5}\times10^{-4}$	$\sim$0.08
Pluto, KC99	0.9%[b]	5×10^{-4}	0.06
Titan	1.5%[c]	4.5×10^{-5}	0.003

L10 and L11 are Lellouch et al. (2010, 2011); KC95 and KC99 are Krasnopolsky and Cruikshank (1995, 1999).

[a] Ratio of the CH_4 and N_2 column abundances.
[b] Model 2 in KC99.
[c] Above the tropopause.

Pluto's atmosphere was studied by stellar occultations in 1988, 2002, and 2006 (Elliot and Young (1992); Elliot et al., 2007, Young et al., 2008); recently the occultation curves from those events were fitted by radiative-conduction models to get basic atmospheric parameters (Zalucha et al., 2011). Search for gaseous species by ground-based high-resolution spectroscopy resulted in detections of CH_4 using CSHELL/IRTF (Young et al., 1997) and CH_4 and CO using CRIRES/VLT (Lellouch et al, 2009, 2011). Middle UV spectroscopy from the Hubble Space Telescope gave only upper limits to C_4H_2, C_6H_2, HC_3N, and C_4N_2 (Krasnopolsky, 2001). These upper limits are $\sim2\times10^{16}$ cm^{-2}, that is, $\sim$5 ppm scaled to an atmosphere of $\sim$10 μbar. The observed CH_4 and CO abundances (Table 4) agree within their uncertainties with those adopted in a photochemical model for Pluto by Krasnopolsky and Cruikshank (1999). Table 4

The supply of H_2O by meteorites is similar near Saturn and Neptune (Feuchtgruber et al, 1997), that is, on Titan, Triton, and probably Pluto. We adopt an H_2O influx of 2×10^6 cm^{-2} s^{-1} for both Triton and Pluto. To account for effects from this water on Triton and Pluto, we compare their photochemistries that are very different despite the similar basic constituents.

7.2. Main features of photochemistry on Triton and Pluto

The CH_4 mole fraction was $\sim10^{-4}$ on Triton during the Voyager flyby. Photolysis by the Lyman-alpha photons from the Sun and the interplanetary background greatly depletes the profile of methane. Ion reactions further reduce CH_4 to $\sim$1 ppm at 200 km (Krasnopolsky and Cruikshank, 1995). Therefore molecular species are scarce in the upper atmosphere, and this gives rise to atomic neutrals N, O, C, and H and atomic ions C^+ and N^+. The observed and calculated densities of N are equal to 5×10^8 cm^{-3} at 200 km with a mole fraction of 0.2%. The slow radiative recombination of atomic ions results in an ionospheric peak density $n_{emax}=3\times10^4$ cm^{-3}, in accord with the Voyager radio occultations (Tyler et al., 1989). Low-energy electrons from the Neptune magnetosphere significantly contribute to the formation of Triton's ionosphere. The CH_4 photolysis peak is at 25 km where the N_2 density is high and facilitates production

of HCN via

$CH+N_2+N_2 \rightarrow HCN_2+N_2$

$HCN_2+H \rightarrow HCN+NH$

Net $CH+H+N_2 \rightarrow HCN+NH$.

These reaction rates are proportional to $[N_2]^2$ near the CH_4 photolysis peak and greatly increase the production of HCN on Triton (Krasnopolsky and Cruikshank, 1995). The detection of HCN in Triton's ice (Burgdorf et al, 2010) confirms this cycle.

Methane is more abundant on Pluto with a mole fraction of 9×10^{-3} at $r=1210$ km in model 2 by Krasnopolsky and Cruikshank (1999). The photolysis and ion reactions are insufficient to deplete this abundant methane and overcome its enrichment by diffusive separation. Hydrocarbon and nitrile chemistries are effective, and production of these species is significant. Atomic nitrogen is diminished to a maximum of 10^5 cm^{-3}, and the ionosphere consists of molecular ions with fast dissociative recombination and a peak density of 800 cm^{-3}, smaller than that on Triton by a factor of 40. The atmospheric structure and photochemistry is affected by a slow hydrodynamic escape (McNutt, 1989; Krasnopolsky, 1999; Strobel, 2008) that was recently questioned by Tucker et al. (2012).

To simulate the transition from the Voyager-type chemistry of Triton to that on Pluto, we calculated vertical profiles of methane on Triton for various CH_4 mixing ratio near the surface. Loss of methane in chemical reactions was interpolated between the models for Triton and Pluto, while the major loss is by photolysis. The results are shown in Fig. 4. The transition between two types of the model occurs near $f_{CH4}\approx5\times10^{-4}$. The CH_4 mole fraction decreases up to 100 km by a factor of $\sim$30 for the smaller values near the surface and is nearly constant for the larger values. Therefore the current Triton with $f_{CH4}\approx2\times10^{-4}$ still keeps the Voyager-type chemistry.

7.3. Results of meteorite supply of H_2O to Triton and Pluto

The meteorite injection of H_2O of $\sim2\times10^6$ cm^{-2} s^{-1} and the subsequent H_2O photolysis on Triton exceed the model production of OH by the reaction of $O+H+M$ by an order of magnitude.

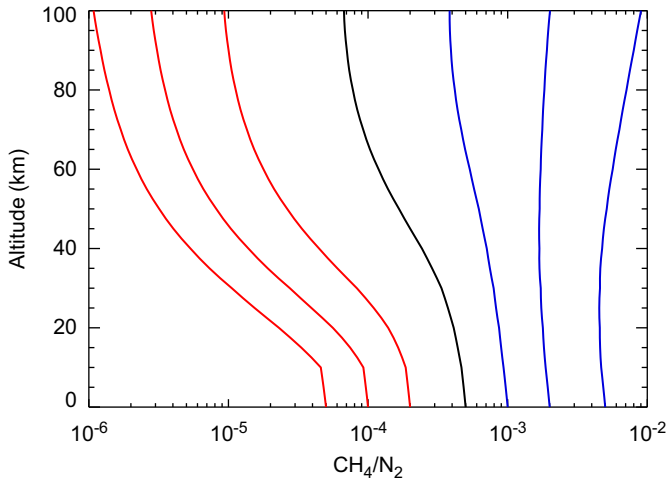

Fig. 4. Calculated profiles of methane mixing ratio on Triton as functions of its ratio near the surface. Photolysis and chemical reactions tend to reduce methane while diffusive separation enhances it. Transition from the atmosphere with large [N] and n_e observed by Voyager to that with low [N], n_e, and abundant hydrocarbons typical of Titan and the current Pluto is at the CH_4 mole fraction of $\sim5\times10^{-4}$ near the surface.

Loss of OH proceeds via

$OH+N \rightarrow NO+H$

$NO+N \rightarrow N_2+O$

Net $OH+2N \rightarrow O+H+N_2$

Production of N is 1.5×10^8 cm^{-2} s^{-1} on Triton, and the appearance of H_2O weakly affects the balance of N. Therefore OH formed by photolysis of H_2O is immediately converted into O that forms CO in reactions with CH_x, CN, and CNN. The production of CO from the meteorite water is larger than its loss by escape of O in the model by Krasnopolsky and Cruikshank (1995) by an order of magnitude, and the meteorite water results in precipitation of $\sim$3 g cm^{-2} Byr^{-1} of CO on Triton. Photolysis of CH_4 with escape of H and H_2 produces some excess of carbon that is partly used to form CO.

For Pluto's atmosphere near perihelion, OH radicals released by photolysis of the injected H_2O react mostly with the abundant CO and form CO_2. Some OH radicals return water in the reaction with CH_3. Photolysis of H_2O is much faster than that of CO_2 (see section 5), and this facilitates the conversion of H_2O into CO_2 that condenses on Pluto.

Pluto's surface temperature is expected to be $\sim$29 K near aphelion at 50 AU, and the N_2 saturated vapor pressure becomes smaller by a factor of $\sim$1000. This huge reduction should significantly affect properties of the atmosphere and its photochemistry.

8. Conclusions

My photochemical model for Titan's atmosphere and ionosphere has been improved using the Troe approximation for termolecular reactions and inclusion of some radiative association reactions from Vuitton et al. (2012). The major improvement of the current model has been achieved by proper fitting of eddy diffusion. This results in a reduction of the mean difference between 63 observed mixing ratios and their calculated values from a factor of 5 in my previous models for Titan to a factor of 3 in the current model.

Oxygen chemistry on Titan is initiated by influxes of H_2O from meteorites and O^+ from magnetospheric interactions with the Saturn rings and Enceladus. Two versions of the model were calculated, with and without the O^+ flux. Balances of CO, CO_2, H_2O, and H_2CO are discussed in detail for both versions. The calculated model with the O^+ flux agrees with the observations of CO, CO_2, and H_2O, including recent H_2O CIRS limb observations and measurements by the Herschel Space Observatory.

Major observational data and photochemical models for Triton and Pluto are briefly discussed. While the basic atmospheric species N_2, CH_4, and CO are similar on Triton and Pluto, properties of their atmospheres are very different with atomic species and ions dominating in Triton's upper atmosphere and ionosphere opposed to the molecular composition on Pluto. Calculations favor a transition between two types of photochemistry at the CH_4 mixing ratio of $\sim5\times10^{-4}$. Therefore Triton's current photochemistry is still similar to that at the Voyager flyby despite the observed increase in N_2 and CH_4. Meteoritic H_2O results in precipitation of CO on Triton and CO_2 on Pluto near perihelion.

References

Banaszkiewicz, M., Lara, L.M., Rodrigo, R., Lopez-Moreno, J.J., Molina-Cuberos, G.J., 2000. A coupled model of Titan's atmosphere and ionosphere. Icarus 147, 386–404.

Broadfoot, A.L., et al., 1989. Ultraviolet spectrometer observations of Neptune and Triton. Science (New York, NY) 246, 1459–1466.

Burgdorf, M., Cruikshank, D.P., Dalle Ore, C.M., Sekiguchi, T., Nakamura, R., Orton, G., Quirico, E., Schmitt, B., 2010. A tentative identification of HCN ice on Triton. The Astrophysical Journal 719, L53–L57.
Conrath, B.J., et al., 1989. Infrared observations of the Neptunian system. Science (New York, NY) 246, 1454–1459.
Cottini, V., et al., 2012. Water vapor in Titan's stratosphere from Cassini CIRS far infrared spectra. Icarus 220, 855–862.
Coustenis, A., Salama, A., Lellouch, E., Encrenaz, T., Bjoraker, G.L., Samuelson, R.E., de Grauw, T., Feuchtgruber, H., Kessler, M.F., 1998. Evidence for water vaporin Titan's atmosphere from ISO/SWS data. Astronomy and Astrophysics 336, L85–L89.
Coustenis, A., et al., 2010. Titan trace gaseous composition from CIRS at the end of the Cassini–Huygens prime mission. Icarus 207, 461–476.
Cravens, T.E., et al., 2005. Titan's ionosphere: model comparison with Cassini Ta data. Geophysical Research Letters 32, L12108. 〈http://dx.doi.org/10.1029/2005GL023249〉.
Cui, J., et al., 2009. Analysis of Titan's neutral upper atmosphere from Cassini Ion Neutral Mass Spectrometer measurements. Icarus 200, 581–615.
De Kok, R., et al., 2007. Oxygen compounds in Titan's stratosphere as observed by Cassini/CIRS. Icarus 186, 354–363.
Elliot, J.L., Young, L.A., 1992. Analysis of stellar occultation data for planetary atmospheres. I. Model fitting, with application to Pluto. The Astronomical Journal 103, 991–1015.
Elliot, J.L., et al., 2000. The prediction and observation of the July 18, 1997 stellar occultation by Triton: more evidence for distortion and increasing pressure in Triton's atmosphere. Icarus 148, 347–369.
Elliot, J.L., et al., 2007. Changes in Pluto's atmosphere: 1988–2006. The Astronomical Journal 134, 1–13.
English, M., Lara, L.M., Lorenz, R.D., Ratcliff, P.M., Rodrigo, R., 1996. Ablation and chemistry of meteoritic materials in the atmosphere of Titan. Advances in Space Research : The Official Journal of the Committee on Space Research (COSPAR) 17, 157–160.
Feuchtgruber, H., Lellouch, E., de Graauw, T., Bezard, B., Encrenaz, T., Griffin, M., 1997. External supply of oxygen to the atmospheres of giant planets. Nature 389, 159–162.
Hartle, R.E., et al., 2006. Preliminary interpretation of Titan plasma interaction as observed by the Cassini Plasma Spectrometer: Comparisons with Voyager 1. Geophysical Research Letters 33, 8201, doi:10.10129/2005GL024817.
Herbert, F., Sandel, B.R., 1991. CH_4 and haze in Triton's lower atmosphere. Journal of Geophysical Research 96, 19,241–19,252.
Hörst, S.M., Vuitton, V., Yelle, R.V., 2008. The origin of oxygen species in Titan'satmosphere. Journal of Geophysical Research 113, E10006, http://dx.doi.org/10.1029/2008JE003135.
Johnson, R.E., Tucker, O.J., Michael, M., Sittler, E.C., Smith, H.T., Young, D.T., Waite, J.H., 2009. Mass loss processes in Titan's atmosphere. In: Brown, R.H., Lebreton, J.P., Waite, J.H. (Eds.), Titan from Cassini-Huygens. Springer, Dordrecht, pp. 373–392.
Kliore, A., et al., 2008. First results from the Cassini radio occultations of the Titan ionosphere. Journal of Geophysical Research 113, A09317. 〈http://dx.doi.org/10.1029/2007/A012965〉.
Krasnopolsky, V.A., 1999. Hydrodynamic flow of N_2 from Pluto. Journal of Geophysical Research 104, 5955–5962.
Krasnopolsky, V.A., 2001. Middle ultraviolet spectroscopy of Pluto and Charon. Icarus 153, 277–284.
Krasnopolsky, V.A., 2009. A photochemical model of Titan's atmosphere and ionosphere. Icarus 201, 226–256.
Krasnopolsky, V.A., 2010. The photochemical model of Titan's atmosphere and ionosphere: A version without hydrodynamic escape. Planetary and Space Science 58, 1507–1515.
Krasnopolsky, V.A., Cruikshank, D.P., 1995. Photochemistry of Triton's atmosphere and ionosphere. Journal of Geophysical Research 100, 21,271–21,286.
Krasnopolsky, V.A., Cruikshank, D.P., 1999. Photochemistry of Pluto's atmosphere and ionosphere near perihelion. Journal of Geophysical Research 104, 21,979–21,996.
Krasnopolsky, V.A., Sandel, B.R., Herbert, F., 1992. Properties of haze in the atmosphere of Triton. Journal of Geophysical Research 97, 11,695–11,700.
Krasnopolsky, V.A., Sandel, B.R., Herbert, F., Vervack, R.J., 1993. Temperature, N_2, and N density profiles of Triton's atmosphere: observations and model. Journal of Geophysical Research 98, 3065–3078.
Lara, L.M., Lellouch, E., Lopes-Moreno, J., Rodrigo, R., 1996. Vertical distribution of Titan's atmospheric neutral constituents. Journal of Geophysical Research 101, 23,261–23,283.
Lavvas, P.P., Coustenis, A., Vardavas, I.M., 2008. Coupling photochemistry with haze formation in Titan's atmosphere. Part II. Results and validation with Cassini/Huygens data. Planetary and Space Science 56, 67–99.
Lellouch, E., Sicardy, B., de Bergh, C., Käufl, H.U., Kassi, S., Campargue, A., 2009. Pluto's lower atmosphere structure and methane abundance from high-resolution spectroscopy and stellar occultations. Astronomy and Astrophysics 495, L17–L21.
Lellouch, E., de Bergh, C., Sicardy, B., Ferron, S., Käufl, H.U., 2010. Detection of CO in Triton's atmosphere and the nature of surface-atmosphere interactions. Astronomy and Astrophysics 512, L8.
Lellouch, E., de Bergh, C., Sicardy, B., Käufl, H.U., Smette, A., 2011. High resolution spectroscopy of Pluto's atmosphere: detection of the 2.3 μm CH_4 bands and evidence for carbon monoxide. Astronomy and Astrophysics 530, L4.
Lutz, B.L., de Bergh, C., Owen, T., 1983. Titan: discovery of carbon monoxide in its atmosphere. Science (New York, NY) 220, 1374–1375.
Magee, B.A., Waite, J.H., Mandt, K.E., Westlake, J., Bell, J., Gell, D.A., 2009. INMS-derived composition of Titan's upper atmosphere: analysis methods and model comparison. Planetary and Space Science 57, 1895–1916.
Marten., A., Hidayat, T., Biraud, Y., Moreno, R., 2002. New millimeter heterodyne observations of Titan: vertical distributions of nitriles HCN, HC_3N, CH_3CN, and the isotope ratio 15N/14N in its atmosphere. Icarus 158, 532–544.
McNutt, R.L., 1989. Models for Pluto's upper atmosphere. Geophysical Research Letters 16, 1225–1228.
Merlin, F., Barucci, M.A., de Bergh, C., DeMeo, F.E., Alvarez-Candal, A., Dumas, C., Cruikshank, D.P., 2010. Chemical and physical properties of the variegated Pluto and Charon surfaces. Icarus 210, 930–943.
Moreno, R., Lellouch, E., Lara, L.M., Courtin, R., Hartogh, P., Rengel, M., 2012. Observations of H_2O in Titan's atmosphere with Herschel. Workshop "Titan Through Time", NASA GSFC.
Moses, J.I., Bezard, B., Lellouch, E., Gladstone, G.R., Feuchtgruber, H., Allen, M., 2000. Phtochemistry of Saturn's atmosphere. I. Hydrocarbon chemistry and comparison with ISO observations. Icarus 143, 244–298.
Niemann, H.B., Atreya, S.K., Demick, J.E., Gautier, D., Haberman, J.A., Harpold, D.N., Kasprzak, W.T., Lunine, J.I., Owen, T.C., Raulin, F., 2010. Composition of Titan's lower atmosphere and simple surface volatiles as measured by the Cassini–Huygens probe gas chromatograph mass spectrometer experiment. Journal of Geophysical Research 115, E12006.
Olkin, C.B., et al., 1997. The thermal structure of Triton's atmosphere: results from the 1993 and 1995 occultations. Icarus 129, 178–201.
Pereira, R.A., Baulch, D.L., Pilling, M.J., Robertson, S.H., Zeng, G., 1997. Temperature and pressure dependence of the multichannel rate coefficients for the CH_3+OH system. The Journal of Physical Chemistry A 101, 9681–9693.
Pollack, J.B., Schwartz, J.M., Rages, K., 1990. Scatterers in Triton's atmosphere: implications for the seasonal volatile cycle. Science (New York, NY) 250, 440–443.
Strobel, D.F., 2008. N_2 escape rates from Pluto's atmosphere. Icarus 193, 612–619.
Strobel, D.F., 2009. Titan's hydrodynamically escaping atmosphere: escape rates and the structure of the exobase region. Icarus 202, 632–641.
Teanby, N.A., Irwin, P.G.J., de-Kok, R., Jolly, A., Bezard, B., Nixon, C.A., Calcutt, S.B., 2009. Titan's stratospheric C_2N_2, C_3H_4, and C_4H_2 abundances from Cassini/CIRS far-infrared spectra. Icarus 202, 620–631.
Toublanc, D., Parisot, J.P., Brillet, J., Gautier, D., Raulin, F., McKay, C.P., 1995. Photochemical modeling of Titan's atmosphere. Icarus 113, 2–26.
Tucker, O.J., Erwin, J.T., Deighan, J.I., Volkov, A.N., Johnson, R.E., 2012. Thermally driven escape from Pluto's atmosphere: a combined fluid/kinetic model. Icarus 217, 408–415.
Tyler, G.L., et al., 1989. Voyager radio science observations of Neptune and Triton. Science (New York, NY) 246, 1466–1473.
Vinatier, S., et al., 2010. Analysis of Cassini/CIRS limb spectra of Titan acquired during the nominal mission. I. Hydrocarbons, nitriles and CO_2 vertical mixing ratio profiles. Icarus 205, 559–570.
Vuitton, V., Yelle, R.V., McEwan, M.J., 2007. Ion chemistry and N-containing molecules in Titan's upper atmosphere. Icarus 191, 722–742.
Vuitton, V., Yelle, R.V., Lavvas, P., Kippenstein, S.J., 2012. Rapid association reaction at low pressure: impact on the formation of hydrocarbons on Titan. The Astrophysical Journal 1, 744, id. 11.
Westlake, J.H., Waite Jr., J.H., Mandt, K.E., Carrasco, N., Bell, J.M., Magee, B.A., Wahlund, J.E., 2012. Titan's ionospheric composition and structure: photochemical modeling of Cassini INMS data. Journal of Geophysical Research 117, E01003. http://dx.doi.org/10.1029/2011JE003883.
Wilson, E.H., Atreya, S.K., 2004. Current state of modeling the photochemistry of Titan's mutually dependent atmosphere and ionosphere. Journal of Geophysical Research 109, E06002, http://dx.doi.org/10.1029/2003JE002181.
Wong, A.S., Morgan, C.G., Yung, Y.L., Owen, T.C., 2002. Evolution of CO on Titan. Icarus 155, 382–392.
Yelle, R.V., Cui, J., Mueller-Wodarg, I.C.F., 2008. Eddy diffusion and methane escape from Titan's atmosphere. Journal of Geophysical Research 113, E10003, http://dx.doi.org/10.1029/2007JE003031.
Yelle, R.V., Vuitton, V., Lavvas, P., Smith, M., Horst, S., Cui, J., 2009. Synthesis of NH_3 in Titan's upper atmosphere. Bulletin of the American Astronomical Society 41, 1023. (abstract).
Young, E.F., et al., 2008. Vertical structure in Pluto's atmosphere from the 2006 June 12 stellar occultation. The Astronomical Journal 136, 1757–1769.
Young, L.A., Elliot, J.L., Tokunaga, A., de Bergh, C., 1997. Detection of gaseous methane on Pluto. Icarus 127, 258–262.
Yung, Y.L., Allen, M., Pinto, J.P., 1984. Photochemistry of the atmosphere of Titan: comparison between model and observations. The Astrophysical Journal Supplement Series 55, 465–506.
Zalucha, A.M., Gulbis, A.A.S., Zhu, X., Strobel, D.F., Elliot, J.L., 2011. An analysis of Pluto occultation light curves using an atmospheric radiative-conduction model. Icarus 211, 804–818.